Metabolic Engineering 78 (2023) 209–222

Contents lists available at ScienceDirect

Metabolic Engineering

journal homepage: www.elsevier.com/locate/meteng

A genome-scale dynamic constraint-based modelling (gDCBM) framework predicts growth dynamics, medium composition and intracellular flux distributions in CHO clonal variations

Mohammadreza Yasemi *, Mario Jolicoeur **

Research Laboratory in Applied Metabolic Engineering, Department of Chemical Engineering, Polytechnique Montréal, P.O. Box 6079, Centre-ville Station, Montréal, Québec, H3C 3A7, Canada

ARTICLE INFO

Keywords:
Mathematical modelling
Genome-scale dynamic constraint-based modelling
Flux distribution
Chinese hamster ovary
Mammalian cell culture

ABSTRACT

Optimizing mammalian cell growth and bioproduction is a tedious task. However, due to the inherent complexity of eukaryotic cells, heuristic experimental approaches such as, metabolic engineering and bioprocess design, are frequently integrated with mathematical models of cell culture to improve biological process efficiency and find paths for improvement. Constraint-based metabolic models have evolved over the last two decades to be used for dynamic modelling in addition to providing a linear description of steady-state metabolic systems. Formulation and implementation of the underlying optimization problems require special attention to the model's performance and feasibility, lack of defects in the definition of system components, and consideration of optimal alternate solutions, in addition to processing power limitations. Here, the time-resolved dynamics of a genome-scale metabolic network of Chinese hamster ovary (CHO) cell metabolism are shown using a genome-scale dynamic constraint-based modelling framework (gDCBM). The metabolic network was adapted from a reference model of CHO genome-scale metabolic model (GSMM), iCHO_DG44_v1, and dynamic restrictions were imposed to its exchange fluxes based on experimental results. We used this framework for predicting physiological changes in CHO clonal variants. Because of the methodical creation of the components for the flux balance analysis optimization problem and the integration of a switch time, this model can generate sequential predictions of intracellular fluxes during growth and non-growth phases (per hour of culture time) and transparently reveal the shortcomings in such practice. As a result of the differences exploited by various clones, we can understand the relevance of changes in intracellular flux distribution and exometabolomics. The integration of various omics data into the given gDCBM framework, as well as the reductionist analysis of the model, can further help bioprocess optimization.

1. Introduction

Mammalian cells have the ability to produce *in vitro* complex biologics of high commercial interest. Successful genetic alterations, growth media optimization, and an effective understanding and management of cellular regulatory mechanisms are expected to yield the next generation of cell factories producing biotherapeutics. Because of their stable growth, high cell density peak, high innate protein expression level, and functional post-translatory regulatory mechanisms, Chinese hamster ovary (CHO) cell lines have been widely used in industry for biotherapeutics manufacturing (Kim et al., 2012). Recombinant CHO cell lines, the gold standard in biotherapeutics production, are responsible for stable and transient protein expressions in bioreactors of various capacities, up to fully monitored production vessels with a working volume of over 20,000 L (Gašperšič et al., 2018). Biotechnological strategies, on the other hand, necessitate extensive quantitative information on cellular metabolism, i.e., establishing a descriptive link between culture conditions and cell productivity. As a result, approaches that provide insight into the flow of carbon, energy, and electrons are extremely desirable because they can quantify metabolic alterations caused by intentional or unintentional perturbations in genetic or environmental factors (Bailey, 1998; Antoniewicz, 2020). Hence,

* Corresponding author.
** Corresponding author.
E-mail addresses: mohammadreza.yasemi@polymtl.ca (M. Yasemi), mario.jolicoeur@polymtl.com (M. Jolicoeur).

https://doi.org/10.1016/j.ymben.2023.06.005
Received 6 July 2022; Received in revised form 16 November 2022; Accepted 9 June 2023
Available online 20 June 2023
1096-7176/© 2023 The Authors. Published by Elsevier Inc. on behalf of International Metabolic Engineering Society. This is an open access article under the CC BY-NC-ND license (http://creativecommons.org/licenses/by-nc-nd/4.0/).

metabolic flux analysis (MFA) is a powerful tool for discovering new bioprocess design solutions that improve the target metabolic product.

Mathematical metabolic models, in combination with high-performance computing and state-of-the-art biomolecules measurement capacity, provides a systems biology approach to describe cell factories, complementing wet-lab methods to improve bioprocess efficiency (Porubsky et al., 2020; Kotidis et al., 2019). On the one hand there is Dynamic Kinetic Modelling (DKM) (Nolan and Lee, 2011; Sha et al., 2018; Cloutier et al., 2009), which requires cell culture experimental data for model kinetic parameters identification, and on the other hand, there is Constraint-based Modelling (CBM) (Varma and Palsson, 1994; Mahadevan et al., 2002; Schellenberger et al., 2011) (reviewed in (Yasemi and Jolicoeur, 2021)), which is based on the stoichiometry of metabolic networks. Metabolic Flux Analysis (MFA) (Quek et al., 2010) and Flux Balance Analysis (FBA) (Orth et al., 2010) are two variants of constraint-based models, each representing determined (or overdetermined) and under-determined metabolic networks, respectively. Without the use of kinetic parameters, these methods can provide credible cell culture models behaviour. The theories that support the validity of FBA provide a fertile ground for the development of more complex approaches for exploring the behaviour of metabolic networks. Flux Variability Analysis (FVA) is one such methodology, in which minimum (and maximum) achievable enzyme activity of each reaction is defined as the objective function, and the flux rates bounds are established by performing linear programming (LP) optimization within the initial problem constraints (Mahadevan and Schilling, 2003). A quadratic minimization of the estimated fluxes is integrated as a bi-level optimization problem in *parsimonious FBA (pFBA)*, on top of the primary objective of FBA, i.e., maximum growth rate (Calmels et al., 2019). In order to switch from descriptive to predictive models, various crucial innovations have come out in the past years. Apart from the more traditional options, such as optimizing growth, researchers have looked into various objective functions for cell functionalities. Indeed, the premise of maximal growth loses its usefulness, especially during the non-growing period or slow growth fed-batch of mammalian cell culture, and other goals such as related to physiological factors and complex proteins processing steps are mostly considered.

The use of CBM extensions to simulate growth and by-products dynamics in non-steady state phases proved being particularly compelling (Varma and Palsson, 1994; Mahadevan et al., 2002). Dynamic Constraint-based Modelling (DCBM) technique is the name given to algorithms with predictive power algorithms developed in this area. In DCBM, the well-known quasi-steady state (QSS) assumption is employed in conjunction with experimental limitations on substrates, oxygen, and energy requirements of growth and production to account for faster intracellular dynamics relative to extracellular matrix dynamics. In this category, there are two ways to follow: sequential and simultaneous methods. The sequential technique, which is used in this study, divides the entire process time into small steps, and the FBA optimization algorithm assumes QSS at each time step, but not at the transition point. The solution to the optimization problem generates new growth and uptake rates, which are then employed in a system of ordinary differential equations (ODEs), whose integration yields in component concentration change over time. If numerous measurement time points are averaged as a single metabolic phase, this method loses information about the real-time evolution of the fluxes. On the other hand, if the time steps are too small, noise in the measured concentrations leads to erroneous uptake rate estimations, and the computing cost becomes a bottleneck. The answer to the optimization problem is obtained in an iterative *static* optimization as long as the unknown fluxes and the objective function are linearly connected. The states dynamics are achieved in this case from the subsequent integral solutions.

Comprehensive experimental research have been conducted to find active metabolic pathways in hybridoma (Savinell and Palsson, 1992; Zupke and Stephanopoulos, 1994, 1995; Xie and Wang, 1996; Bonarius et al., 1996) and then in CHO cell lines (Nyberg et al., 1999; Altamirano et al., 2001, 2006), for developing pre-genomic structured metabolic networks. Subsequent investigations of CHO (Zamorano et al., 2010; Fernandes de Sousa et al., 2016) enlarged these bioreaction networks from a set of less than fifty biological reactions to include a more thorough metabolism of amino acids and nucleotides, including roughly 100 reactions. After the publication of the first genome-wide metabolic model of CHO in 2011 (Hammond et al., 2011), and a consensus community-based CHO genome-scale model in 2016 (Hefzi et al., 2016), new opportunities for metabolic modelling of CHO cell cultures have emerged. Some recent studies on CHO metabolism (Yeo et al., 2020; Calmels et al., 2019; Széliová et al., 2020) addressed revising the consensus GSMM for constructing context-specific metabolic models. In fact, multiple approaches for extracting consistent metabolic models from the reduction of GSMMs have been derived, each based on distinct assumptions and screening criteria for including the content of a reference GSMM (Ataman et al., 2017; Erdrich et al., 2015; Lugar et al., 2021). These metabolic model extraction methods provide a crucial computational toolkit for extracting context-specific metabolic models from an organism's most comprehensive metabolic model. Other omics data, such as exometabolomics or transcriptomics data, may be used in computational algorithms for designing GSMMs (Becker and Palsson, 2008; Pacheco and Sauter, 2018). Other frequent requirements include establishing a list of preserved metabolites and reactions, as well as requiring the reduced model to perform specific metabolic tasks (Richelle et al., 2019). Furthermore, the complexity of eukaryotic cells necessitates considerations of compartmentalization, metabolic process energetic costs, and biomass composition.

Here, we revised a recent GSMM of CHO (Calmels et al., 2019), as deposited on http://bigg.ucsd.edu/models/iCHOv1_DG44 (mat file), as the metabolic network for developing a gDCBM model of a bioprocess. The underlying metabolic network was built and then the corresponding stoichiometric matrix was determined to be used in the main optimization problem that is subsequently formulated. A smoothing spline fit was performed on exometabolomics to convert the raw experimental data from three strains of CHO to dynamic exchange flux bounds. The data corresponds to parental, low-producing and high-producing CHO strains that have been described in a previous study (Ghorbaniaghdam et al., 2014). The gDCBM framework is consequently used for modelling and the results are discussed.

2. Methods

2.1. Metabolic network development

We selected the model contributed in (Calmels et al., 2019) because the authors updated the consensus GSMM (Hefzi et al., 2016) by considering the gene expression data in CHO_DG44 by applying Gene Inactivity Moderated by Metabolism and Expression (GIMME) algorithm (Becker and Palsson, 2008). In a preliminary analysis using swiftcore algorithm (Tefagh and Boyd, 2020), we realized that 470 metabolites out of 2750 are dead-ends and 1810 out of 3942 reactions are inconsistent, i.e., unable to carry metabolic flux under any conditions. Thus, the network was reduced by removal of such nonfunctional components. The configurations of our stoichiometric model used throughout the next sections is given in Table 1 and the complete list of the reactions is

Table 1
Comparison of the original and curated genome-scale metabolic models.

	Initial model	Curated model
Number of reactions	3942	2123
Number of blocked reactions	1819	0
Number of balanced reactions	3211	1931
Number of metabolites	2751	1285
Number of dead-end metabolites	470	0
Number of extracellular metabolites	580	226

given in the supplementary material file (Reactions List).

hhe2.2. Phenomenological reactions

Here, the phenomenological reactions are particularly referring to the net biochemical transformations represented as a single (pseudo-) reaction. The scope of the metabolic network requires assuming the following (pseudo-) reactions.

2.2.1. Biomass synthesis

The biomass synthesis reaction directly affects predictions for *in silico* cell growth and maintenance. The weight fractions for the cell building blocks, i.e., lipids, proteins, DNA, RNA, and carbohydrates, with respect to the cell dry mass, molar fractions of the macromolecular building blocks, macromolecules average molar weights and CHO_DG44 dry mass weight were all taken from (Széliová et al., 2020), ID/DGpar-8mMCD. In (Széliová et al., 2020) flux units are different than this study ($mmol\ gDW^{-1}\ h^{-1}$ vs. $nmol\ 10^{-6} cell\ h^{-1}$), therefore, we converted the stoichiometric coefficients accordingly. Then the cell components synthesis reactions were lumped to form the biomass synthesis reaction. Finally, the original BIOMASS_cho_producing_1 reaction in iCHOv1_DG_44 was replaced by the new reaction. The calculation details are given in the supplementary material files (Biomass_eqn_1 and Biomass_eqn_2). We named this reaction MY_BIOMASS_cho_producing_1 for distinction.

2.2.2. Antibody production

In the experimental study, Ghorbaniaghdam et al. (2014) proposed a model mAb against CD20 protein, we assumed this mAb has the same amino acid sequence as Rituximab (*Mabthera®*) (Aoyama et al., 2018) the most similar commercial human mAb. Then, the amino acid sequence for light- and heavy-chains and an average molecular mass of 143.86 (*g/mmol*) were retrieved from (type). The antibody production reaction was developed based on the procedure used in (Szeliova et al., 2021). The polymerisation energy demand was coupled to the reaction by inclusion of 2 GTP and 1.306 ATP hydrolysis to 2 GDP, 1 AMP and 0.306 ADP per peptide bound formed (Sheikh et al., 2005). Thus, the balanced reactions specific to Rituximab heavy-chain and light-chain replaced reactions *igg_hc_1* and *igg_lc_1* in iCHO_v1_DG44, respectively, and the *igg_formation* reaction remained intact. The detailed calculations are given in the supplementary material file (mAb_eqn).

2.2.3. Energetic requirements

We considered the growth-associated and non-growth associated energy consumption for the cell maintenance (mATP). The growth-associated maintenance ATP consumption was included in the biomass synthesis reaction after lumping the macromolecular biosynthesis reactions. As such, −1360 (*nmol*) ATP and −2000 (*nmol*) GTP is hydrolyzed for synthesis of 10^6 cells. To account for the non-growth associated maintenance ATP, for example due to membrane leak or protein turnover costs, we used the estimated values in a recent study on the impacts of mATP inclusion on the intracellular flux predictions (Szeliova et al., 2021). Particularly, we used the estimated values for (Sheikholeslami et al., 2013, 2014), which have similar conditions with the Ghorbaniaghdam et al. (2014). Thus, we imposed a lower bound of 718.2 ($nmol\ 10^{-6} cell\ h^{-1}$) (equal to 3.6 ($mmol\ gDW^{-1}\ h^{-1}$)) on the mATP reaction.

2.2.4. Oxidative stress termination

Reactive oxygen species (ROS) are produced when there is (even partly) aerobic metabolism involved. We used the lumped reaction 2.0 gthrd_c + 3.0 h2o2_c → gthox_c + 4.0 h2o_c + o2_c (Calmels et al., 2019) to represent H2O2 termination.

2.3. Defining metabolic network stoichiometric matrix

The tailored CHO metabolic network transforms into a stoichiometric matrix that maps intracellular and transport reactions (between the cytosol and the external environment) to intracellular and extracellular metabolites dynamic of change, i.e. mass balances. As a result, the stoichiometric matrix (and metabolic fluxes vector) were partitioned as shown in the equation below.

$$\frac{\overrightarrow{\Delta Z_{bal}}}{\Delta t} = S_{bal}\overrightarrow{v} = [S_{II} \quad S_{IT}]\begin{bmatrix}\overrightarrow{v_{Int}}\\ \overrightarrow{v_{Tr}}\end{bmatrix} = \overrightarrow{b_m} \tag{1}$$

$$\frac{\overrightarrow{\Delta Z_{nbal}}}{\Delta t} = S_{nbal}\overrightarrow{v}X = [S_{EI} \quad S_{ET}]\begin{bmatrix}\overrightarrow{v_{Int}}\\ \overrightarrow{v_{Tr}}\end{bmatrix}X = \overrightarrow{r_l}X, \tag{2}$$

where $Z_{bal} \in \mathbb{R}^m$ and $Z_{nbal} \in \mathbb{R}^l$ are the concentrations of intracellular and extracellular metabolites respectively in ($nmol/10^6 cell$) and ($\mu mol/litre$). The vector v represents specific fluxes in ($nmol/10^6 cell/hr$) with dimension n, divided into transport fluxes ($\overrightarrow{v_{Tr}}$) and intracellular fluxes ($\overrightarrow{v_{Int}}$). The stoichiometric matrix S of dimension $(m + l) \times n$ is divided into S_{II} (intracellular metabolite to intracellular reaction), S_{IT} (intracellular metabolite to transport reaction), $S_{EI} = 0$ (extracellular metabolite to intracellular reaction) and S_{ET} (extracellular metabolite to transport reaction). The row decomposition is used in the calculations to distinguish between the metabolites for which the steady state assumption is imposed (S_{bal}), or not (S_{nbal}). Thus, the vectors b_m and r_l present the associated accumulation rates. Based on the QSS, vector b_m equals zero (Stephanopoulos et al., 1998).

2.4. Formulating constrained optimization problem of gDCBM

We defined the dynamic optimization problem in the form of a differential-algebraic equation (DAE). Thus, the main problem is formulated in Equations (3-12).

$$\max_{\overrightarrow{v(t)},\overrightarrow{Z(t)},X(t)} \quad \alpha J_1 + \beta J_2 \tag{3}$$

$$\text{Subject to} \quad \frac{\overrightarrow{\Delta Z_{bal}}}{\Delta t} = 0 \tag{4}$$

$$\overrightarrow{r_l^{lb}} \le \frac{\overrightarrow{\Delta Z_{nbal}}}{\Delta t} \le \overrightarrow{r_l^{ub}} \tag{5}$$

$$\frac{\Delta X}{\Delta t} = \mu . X(t) \tag{6}$$

$$\mu = MY_CHO_Biomass \tag{7}$$

$$t_j = t_0 + j\frac{t_f - t_0}{N_{ts}}, \qquad j = 0, .., N_{ts}, \qquad \frac{t_f - t_0}{N_{ts}} = 1(hr) \tag{8}$$

$$\alpha = \begin{cases} 1, & \text{if} \quad t \le t_{switch} \\ 0, & \text{otherwise.} \end{cases}, \qquad \beta = 1 \tag{9}$$

$$Z \ge 0 \quad X \ge 0 \qquad \forall t \in [t_0, t_f] \tag{10}$$

$$Z(t_0) = Z_0 \quad X(t_0) = X_0 \tag{11}$$

$$lb \le v \le ub, \qquad \forall t \in [t_0, t_f] \tag{12}$$

Where J_1 and J_2 in Equation (3) are the objective functions, α and β are the corresponding weightings. Equation (4) represent the QSS assumption, and r_l^{lb} and r_l^{ub} denote the bounds on the measured cell specific uptake rates (explained in the next section). μ is the growth rate equal to the rate of MY_CHO_Biomass reaction. t_j represents the descretized time points, moreover, N_{ts} is chosen as such the time interval between simulation points is equal to 1 h. In Equation (9), t_{switch} was determined to minimize the fit error measurement. The non-negativity constraint is imposed on the metabolite and cell concentrations. in Equation (11), the initial concentrations are assigned based on the

experimental data. Finally, each flux value v is bounded by a lower bound (lb) and an upper bound (ub) (Thiele and Palsson, 2010).

The objective functions for the above optimization problem is detailed in Equations (13) and (14).

$$J_1(\vec{v}, \overrightarrow{Z_{nbal}}, X) = \mu(t)|_{t<t_{switch}}, \qquad \text{growth dependent}, \tag{13}$$

$$J_2(\vec{v}, \overrightarrow{Z_{nbal}}, X) = \sum_{j=1}^{N_{sf}} -v_j, \qquad \text{growth independent} \tag{14}$$

J_1 is the assumption of the growth rate maximization at any given time, which is valid before the switch to the non-growth phase. J_2 is the uptake rate objective functions which were defined for a subset N_{sf} of amino acids. We hypothesize that since it is a nutrient-rich environment, the goal of the cell is to maximize utilization of resources, and not to minimize nutrient consumption (Chen et al., 2019). We included EX_gln_L_e, EX_val_L_e, EX_ala_L_e, EX_tyr_L_e, EX_phe_L_e, EX_met_L_e, EX_leu_L_e, EX_his_L_e, EX_arg_L_e, EX_cys_L_e, which are the exchange reactions for the associated metabolites. We chose the metabolites that would decrease the prediction error measurement, other metabolites would either worsen the fit or do not change it. Therefore, the optimization has multiple objectives when it comes to the non-growth phase.

2.5. Metabolomics data integration as exchange flux bounds

The data for this study was collected from six out of ten batch studies, including two parental, two low-producing, and two high-producing batch cell cultures, and eliminating two induced low-producing, two induced high-producing batch cell cultures (Ghorbaniaghdam et al., 2014). We excluded the induced data sets because, first, the analysis in the original paper showed that induction does not cause significantly different behaviour (in the defined experimental conditions), and second, the pseudo-steady state assumption is likely to fail where a dramatic transient is expected, such as in transcription factor induction (Quek et al., 2010), resulting in gross model error. Measurements for glucose, lactate, ammonium (3), amino acids (14), CD-20 (1), oxygen uptake rate (1), and cell concentration (1) are included in the three data sets (in duplicates) of non-induced cultures. The data spans growth and non-growth stages, from seed culture inoculation until the end of the sixth day (144 h), when viability decreases below 70%. To determine exchange fluxes for constraining the model, the following method was adapted.

2.5.1. Spline fitting of the exometabolomics and framing uncertainty in the concentration measurements

Because metabolomics data is often noisy and sparse, two challenges arise when such data is differentiated to compute exchange fluxes. First, the computed results are non-smooth, and second, the calculated exchange fluxes are erroneous because they do not account for the inherent uncertainty of experimental measurements. Thus, imposing exact values for individual uptake fluxes is prone to inaccuracy and considerably increases infeasibility issues. We used zero mean standard noise with a standard deviation twice the experimental value to populate the experimental data, and then piece-wise cubic spline functions to fit the measured concentrations. The numerical derivatives of the evaluated fit functions were then calculated to produce a range of specific uptake rate values (r_l^{lb} and r_l^{ub}) as imposed by Equation (5). The exchange fluxes were constrained at each time point using the maximum fitting uptake or secretion rates.

$$PP_i = f(t, Z_{nbal,i}, p) \tag{15}$$

$$r_i = \frac{dPP_i}{dt} \tag{16}$$

where PP_i is the piece-wise polynomial fit on the $Z_{nbal,i}$ at time t, and p is the estimated spline parameters. $\frac{dPP_i}{dt}$ is the numeral derivative representing specific uptake rates r_i.

2.6. Sequential dynamic optimization

The optimization problem in Equation (3-12) contains both algebraic and differential equation models that makes its simultaneous solution impossible for LP solvers. It can be solved either as a nonlinear programming (NLP) problem and by methods such as orthogonal collocations on finite elements, or as LP problems solved and integrated sequentially (Cuthrell and Biegler, 1987; Mahadevan et al., 2002). The sequential solution of the problem is used here, the procedure involves discretizing a scalar dimension (time), into a set of intervals, i.e., $t_{j+1} - t_j$ that suffice error minimization, and converting the differential equations to a set of approximating algebraic equations, which are then integrated to yield the states trajectories.

2.7. Identifying the range of alternate optima for intracellular flux predictions

We did FVA at each of the simulation time points and after the main optimization problem was solved to identify the intracellular flux ranges based on the solution of $2n$ number of LP problems (n being the number of reactions) optimizing for min/max of each reaction flux (Mahadevan and Schilling, 2003). The default information on reversibility/irreversibility was based on the iCHOv1_DG44_v1 flux bounds.

$$\min_{\vec{v} \in \mathbb{R}^n} / \max f(\vec{v}) \qquad := v_i \qquad v_i \in \begin{bmatrix} \overrightarrow{v_{Intra}} \\ \overrightarrow{v_{Transport}} \end{bmatrix} \tag{17}$$
$$\text{Subject to} \qquad \text{Equation}(3-12);$$

2.8. Prediction error measurement

To measure the prediction error, we used the following normalized root mean squared error (NRMSE) formula (Gábor and Banga, 2015),

$$NRMSE = \sqrt{\frac{1}{N_D} \sum_{k=1}^{N_e} \sum_{j=1}^{N_{y,k}} \frac{\sum_{i=1}^{N_{t,k,j}} (y_{ijk} - \widetilde{y}_{ijk})^2}{(\max_i \widetilde{y}_{ijk} - \min_i \widetilde{y}_{ijk})^2}} \tag{18}$$

Here N_D is the total number of data points for 18 observables, N_e is the number of experiments, $N_{y,k}$ is the number of observables in the k-th experiment, $N_{t,k,j}$ is the number of time points in the k-th experiments for the j-th observable. y_{ijk} is the model prediction for the data $\widetilde{y}_{ijk}$. This formula computes the root of the sum of squared error between model prediction and data for each observable, and normalizes it by the squared range of the data corresponding to that observable. Thus, the observables are properly scaled.

3. Results and discussions

3.1. Development of a genome-scale dynamic constraint-based modelling (gDCBM) framework

DCBM techniques were used to provide a modular framework for evaluating CHO dynamic metabolism in batch cell cultures with CHO clonal variants in this study. As shown in Fig. 1, the framework starts with a set of conventional cell culture data and a reference GSMM. The output includes time-resolved dynamics of medium components (mostly amino acids) and intracellular flux distributions with the alternate optima range of the fluxes. We demonstrated that this approach may be used to predict cell culture dynamics without the necessity for biosystem kinetic data.We upgraded the CHO GSMM by removing the blocked reactions and changing the phenomenological reactions to fit the

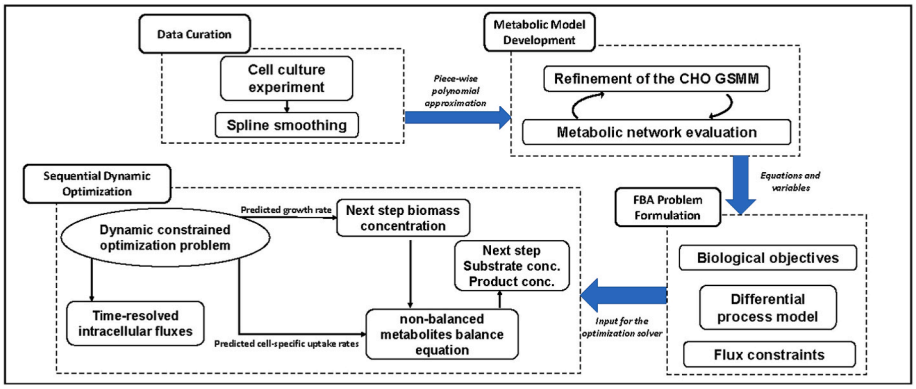

Fig. 1. The gDCBM framework Four interactive components make up the framework. Smooth splines are used to approximate the data in the first module. The metabolic model is developed from the reference GSMM in the second module, while dynamic limitations imposed by the piece-wise polynomials formed in the data curation module are taken into account. The body of the FBA problem is formulated in the third module, and we employ optimization solvers to derive the final answers in the fourth module.

demands of the investigation. The traditional application of the molar mass conservation rule is challenging and expensive due to the unprecedented complexity and uncertainty of biomass composition. Based on a recent detailed assessment of CHO biomass composition in various strains as explained in the Methods section (2.2.1), we elected to create a standard version of the model with a biomass synthesis reaction. To investigate nutrient metabolism in CHO cells, we looked at three different types of growth medium components. For each category, the gDCBM predictions of extracellular metabolites are presented alongside the experimental results in the accompanying figures.

1. The main metabolites: glucose (GLC), lactate (LAC), glutamine (GLN) and ammonia (NH4).
2. The nonessential amino acids: alanine (ALA), arginine (ARG), cysteine (CYS), glutamate (GLU), glycine (GLY), serine (SER), tyrosine (TYR).
3. The essential amino acids: histidine (HIS), isoleucine (ILE), leucine (LEU), methionine (MET), phenylalanine (PHE), valine (VAL).

3.2. The gDCBM framework accommodates a posteriori determination of the switch time

The switch time linked with each clone was calculated by looking for the time point with the least NRMSE. For the different clones, the exercise resulted in three different switch time points. The parental clone demonstrated a late switch, followed by a fall in cell viability, as is common in mammalian cell culture, whereas the high-producer clone converted to non-growth phase as early as 71 h after inoculation. In every example, the gDCBM predictions are very close to the experimental results. Indeed, we demonstrated that the framework allows for *a posteriori* determination of the transition from growth to non-growth phase based on the reduction of the NRMSE, which accounts for the prediction versus experimental data mismatch among all observable states.

3.3. The assumption of varying protein content of the cell

Because the initial cell composition was assessed in a producing cell line, the derived biomass synthesis reaction predicted the high-producing clone with the least error compared to the other two clones. We discovered that the biomass synthesis reaction results in a considerable underestimating of the growth rate for low-producer and parental clones in our preliminary simulations. We hypothesised that the disagreement stemmed from differences in clone amino acid compositions, thus we calculated a multiplier for the amino acid coefficients in the cell biosynthesis reaction. Thus, the reaction coefficients of the 18 amino acids involved in biomass synthesis (MET, ASN, CYS, GLN, SER, THR, ARG, GLY, PHE, GLU, ASP, VAL, TRP, TYR, HIS, LEU, ILE, and LYS) were multiplied by a factor of 0.7 and 0.9, resulting in the protein content for parental and low-producer, respectively. The modification is based on the notion that the cell makeup of the clones varies, which is supported by literature (Feist and Palsson, 2010). This adjustment is required to accommodate changes in cell lines, and it only needs to be done once; the coefficients will remain fixed after that. Another consequence of the modification is that, in the absence of kinetic parameters, amino acid biomass synthesis coefficients emerged as a significant source of sensitivity.

3.4. The gDCBM approach with uptake rates as objective functions predicts medium composition dynamics

The growth optimization assumption is based on the output of cellular activity, and while it leads to successful *in silico* results (especially for organisms simpler than mammals), it loses relevance in the non-growth phase and must be replaced by other objective functions to meet the necessary conditions of an optimization problem formulation. Moreover, further proof that a cell can design optimal behaviour for more than one metabolic objective (Schuetz et al., 2012) begs the question of what those objectives could be and how important they are in determining cell behaviour. In contrast to the limited nutrient consumption assumption (Chen et al., 2019), we assume that in a rich cell culture media, CHO cells attempt to ingest as many nutrients as their internal metabolism allows and secrete as much product as their internal metabolism determines. As a result, we focus on the cell's input and presume that intracellular activity is the limiting factor in the exchange of medium constituents across the cell membrane. These substances' input flows can be used as objectives in the primary FBA optimization problem. We were able to acquire the simulations in Figs. 2, 4 and 6 owing to this approach. We hypothesised a maximum intake of 10 amino acids, as outlined in the Method section. This systemic synthesis of numerous important biological objective functions, followed by model-driven analysis of the resulting flux distribution optima, could provide a viable computational technique for systems-level inspection of context-specific metabolic behaviour. If the individual fluxes had not been restricted previously by the derivative of the fitted cubic splines, the procedure would fail, highlighting the importance of following order of the modules in the framework application (see Fig. 5) (see Fig. 3).

The results are analysed to establish the limitations of the culture media that may have contributed to the cell decline or switch from growth to non-growth. Overfeeding glucose slows lactate uptake, and this combination of glucose and glutamine feed is not optimal, resulting in a non-optimal metabolism in which a considerable percentage of glucose is converted to lactate, while glutamine is rapidly consumed, especially in the producing cell line. However, both ammonia and lactate remain below lethal levels, leading us to believe that the switch to non-growth phase is caused by a glutamine shortage. The clonal diversity had no effect on cell survival or concentration until the metabolic switch to the non-growth phase, although the peak cell density in the

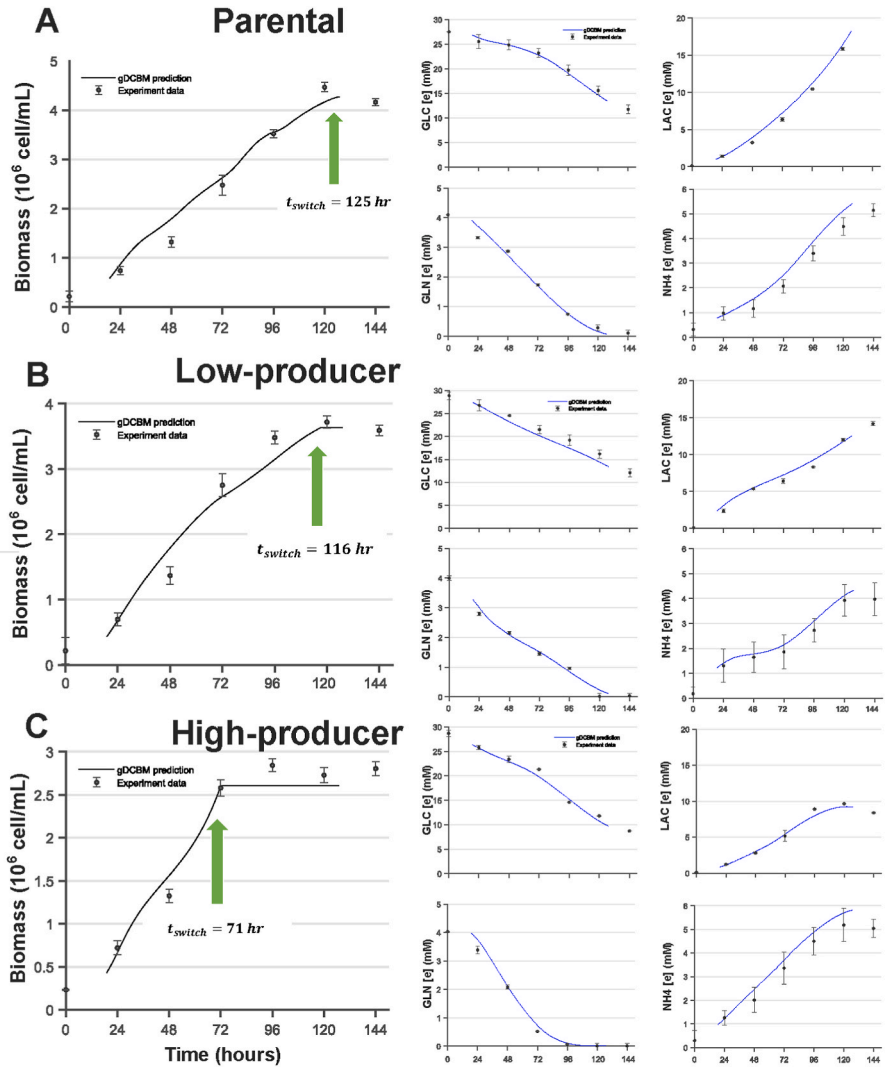

Fig. 2. Cell growth and concentrations of the extracellular metabolites: Main metabolites The growth dynamics is on the left and the concentrations dynamics are on the right for GLC, GLN, LAC and NH4. The green arrow indicates the switch time from the growth to non-growth phase.

high-producer clone is significantly lower.

In the production phase of the high-producer, HIS, ILE, and MET depleted from the essential amino acids which may have caused a reduction in the monoclonal antibody. The depletion does not happen in the other two clones, however, the mentioned amino acids remain available in small amounts. For the non-essential amino acids, we observe depletion of SER and TYR especially in the high-producer clone. Most probably either higher initial concentrations or intermediate feeding of the mentioned five amino acids could fuel cell metabolism to produce more antibody. Interestingly, the model captures the metabolic shift from alanine production to alanine consumption accurately with the most pronounced shift for the high-producer clone.

3.5. Solution space underdeterminancy and infeasibility

We know that the biosystem acquires a mass balanced carbon flux distribution at the experimental conditions, thus, we expect the model to find feasible solutions within the same *in-silico* conditions. We argue that if the LP optimization solver cannot find a feasible solution in the flux vector space $\mathbb{R}^n$, then, there exist some limitations in the model such as unfilled gaps, inaccurate mechanistic assumptions, inconsistent model scope, etc. Relaxations in the imposed exchange fluxes to account for the exometabolomics uncertainty and resolving conflicting equations by modifying metabolic network connectedness both reduced the infeasibility. After we have had adequate experience with the preliminary model simulations, we differentiated between relaxations and conflicting equations. We addressed the former by adopting spline smoothing method followed by constraints from one way for the exchange fluxes and the latter by tailoring the network to remove blocked reactions and modifying bounds on the remaining reactions. Hence, both these items play important roles in tackling the infeasibility issue regularly associated with stoichiometric-based models ((Meadows et al., 2010; Nolan and Lee, 2012)). We used COBRA Toolbox library functions to check for the consistency of reactions, carbon balance, removal of blocked reactions and frameworking computations.

It is shown in Fig. 7 that HIS and ILE are consumed more rapidly during the growth-phase of the high-producer clone. This could suggest that production begins prior to the transition to the non-growth phase. In the case of ILE, the simulation matches experimental data when practically all consumption in the non-growth interval ceases. Unlike the parental and low-producer clones, the high-producer clone's intake of LEU, MET, and PHE remains stable until the end of the culture time. Notable is also the fact that, at least for LEU, PHE, and VAL, the consumption rate in the majority of culture time points is far from the estimated limit value, demonstrating the efficacy of our method in viewing the specific rates as a range rather than a single value.

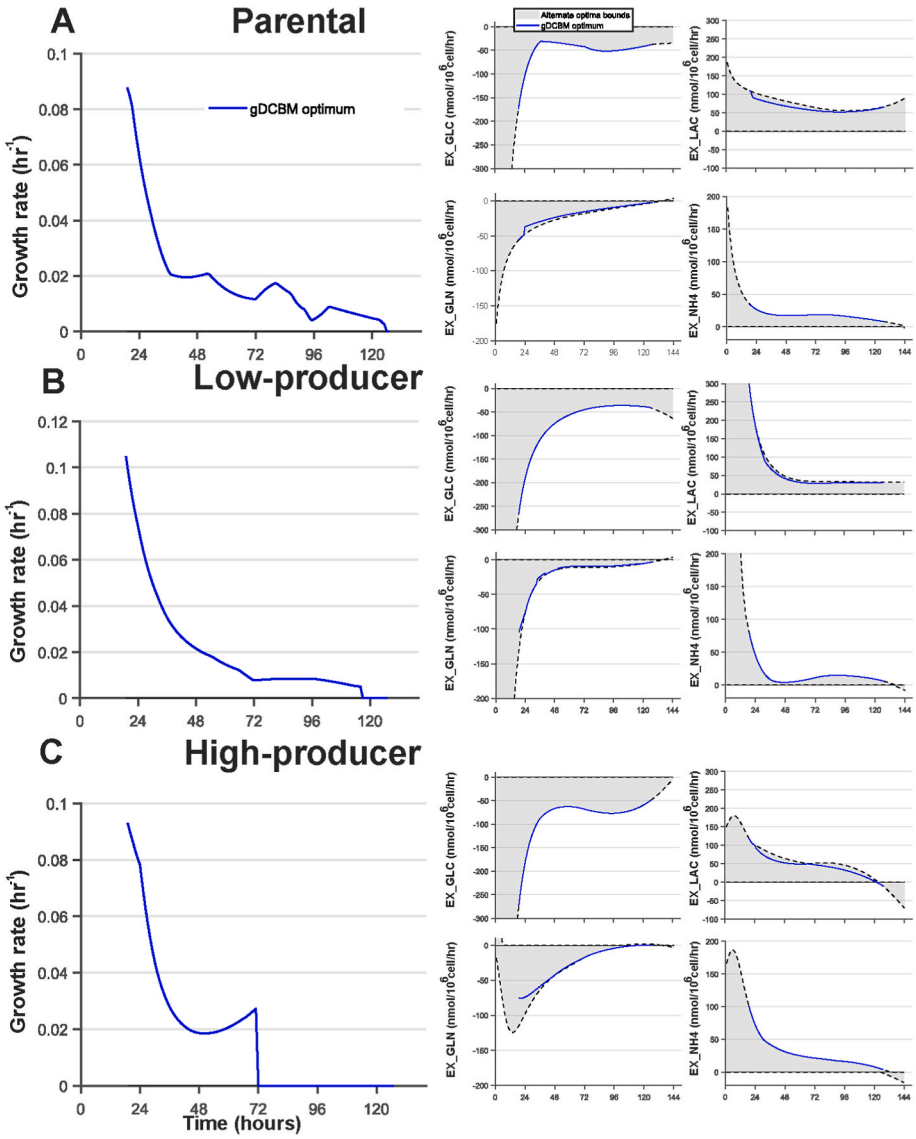

Fig. 3. Growth rate and specific uptake or secretion rates: Main metabolites The instantaneous growth rates are on the left and the specific rates are on the right for EX_GLC, EX_GLN, EX_LAC and EX_NH4 for the parental **(A)**, low-producer **(B)**, and high-producer **(C)** clones. The shaded area shows allowed bounds for the specific rates and the blue line represents the gDCBM predictions.

3.6. Indicators of increased efficiency

It is known that high-producing cell lines have a higher efficiency in carbon utilization than non-producing cell lines. In our simulations, the model can capture the differences between the global metabolism of clones. For example, in Fig. 2 comparing panel A and panel C shows that lactate is produced much less in high-producer clone compared to the parental and low-producing cell lines and even the high-producer starts consuming lactate at the end of the cell culture. Similar trend with a more pronounced uptake is observed for alanine, which is continuously produced even after the glutamine consumption in the parental cell culture but it is consumed in the high-producer when glutamine is depleted. We hypothesize that the cellular control machinery will expend energy to create (or activate) a pathway for utilization of the less favorable nitrogen source and in return the cell productivity is sustained.

3.7. Comparison between clones with different mAb productivity levels

We argue that understanding the cellular physiology dynamics during the cell culture is the key to creating high-producing cell lines. The flux magnitude of model antibody production is relatively small when compared to the flux value through biomass synthesis, thus, the productivity level does not have a considerable impact on flux prediction results. However, the fact that a clone is engineered to be a high-producer rewires its metabolism. There are puzzling areas of CHO metabolism that obstacle harnessing an efficient energy metabolism for achieving yields closer to the theoretical production yields. The results show that glucose and glutamine are the primary sources for energy and carbon skeleton, depletion of each of which resulting in the growth limitation. Moreover, the time-resolved dynamics of asparagine, alanine, glycine and glutamate shows distributed nitrogen source utilization throughout the culture, especially after glutamine is depleted. Based on the results provided here, it seems that glucose must be fed in minimal amounts as this has advantages both for the limitation of undesired Warburg effect and possible commence of substrate utilization for product formation rather than growth maximization. Interestingly, even though nitrogen intake increased in the high-producer, the waste *NH4* did not exceed its levels in the parental and low-producer clone. It shows that the increase in nitrogen consumption encountered with an

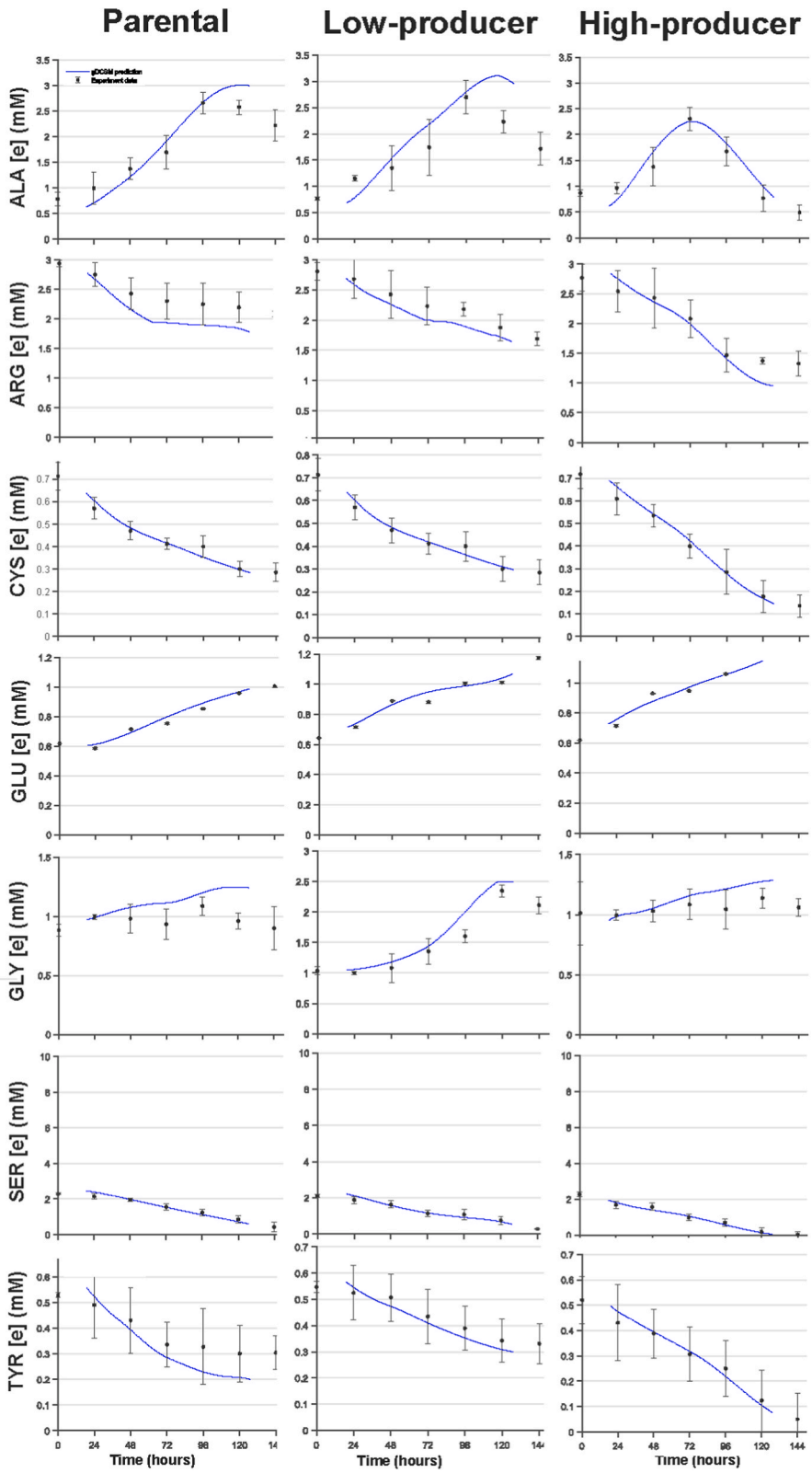

Fig. 4. Concentrations of the extracellular metabolites: Non-Essential amino acids The rows reflect non-essential amino acid concentrations for which measurements were obtained, and the columns represent parental, low-producer, and high-producer clones. The blue lines reflect the gDCBM prediction of the concentrations, while the error bars reveal the experimental data.

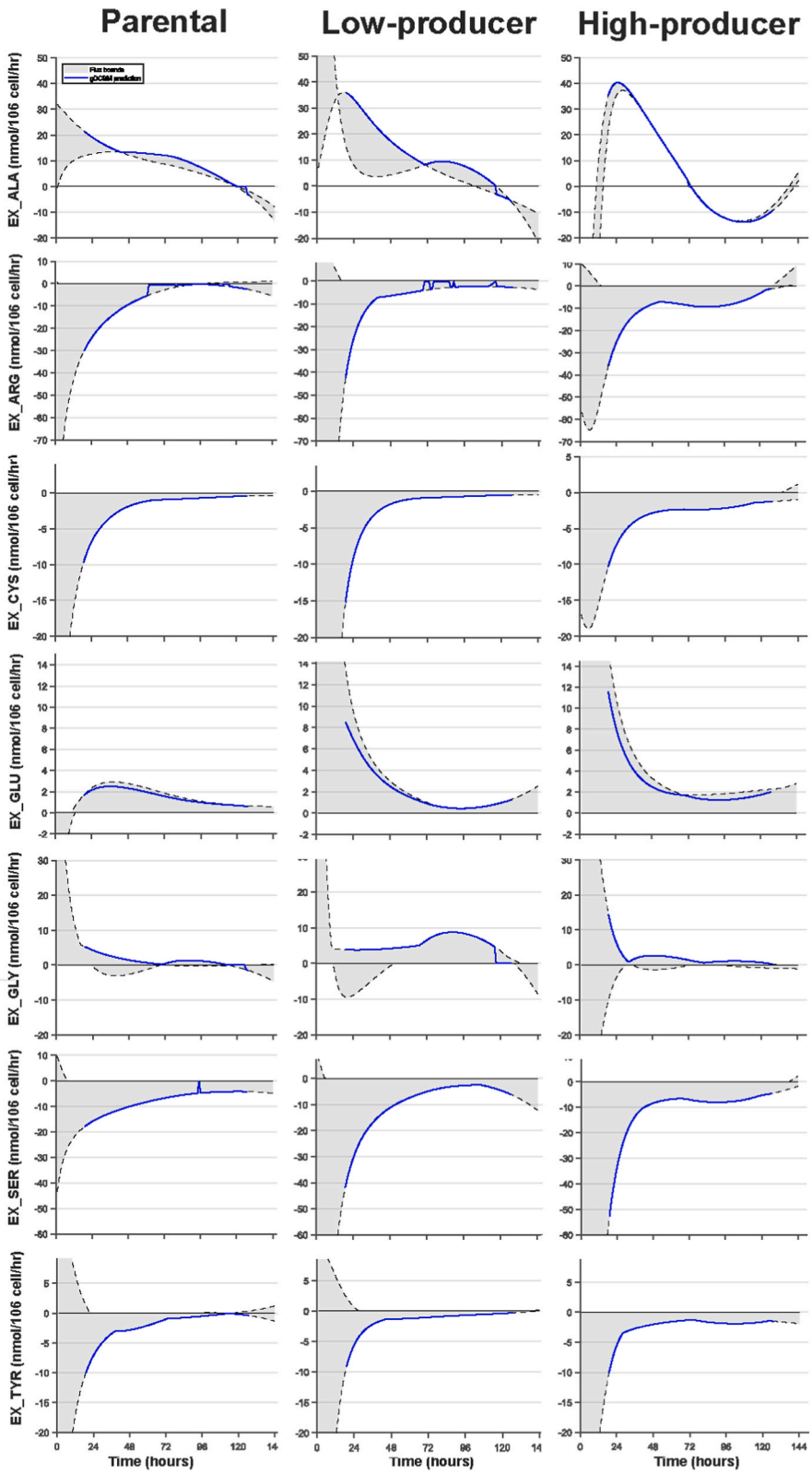

Fig. 5. Specific uptake or secretion rates: Non-Essential amino acids The columns correspond to the parental, low-producer, and high-producer clones, respectively, and the rows to non-essential amino acids for which measurements were available. The blue lines reflect the gDCBM prediction of the specific rates, while the shaded areas show allowed bounds for the specific rates.

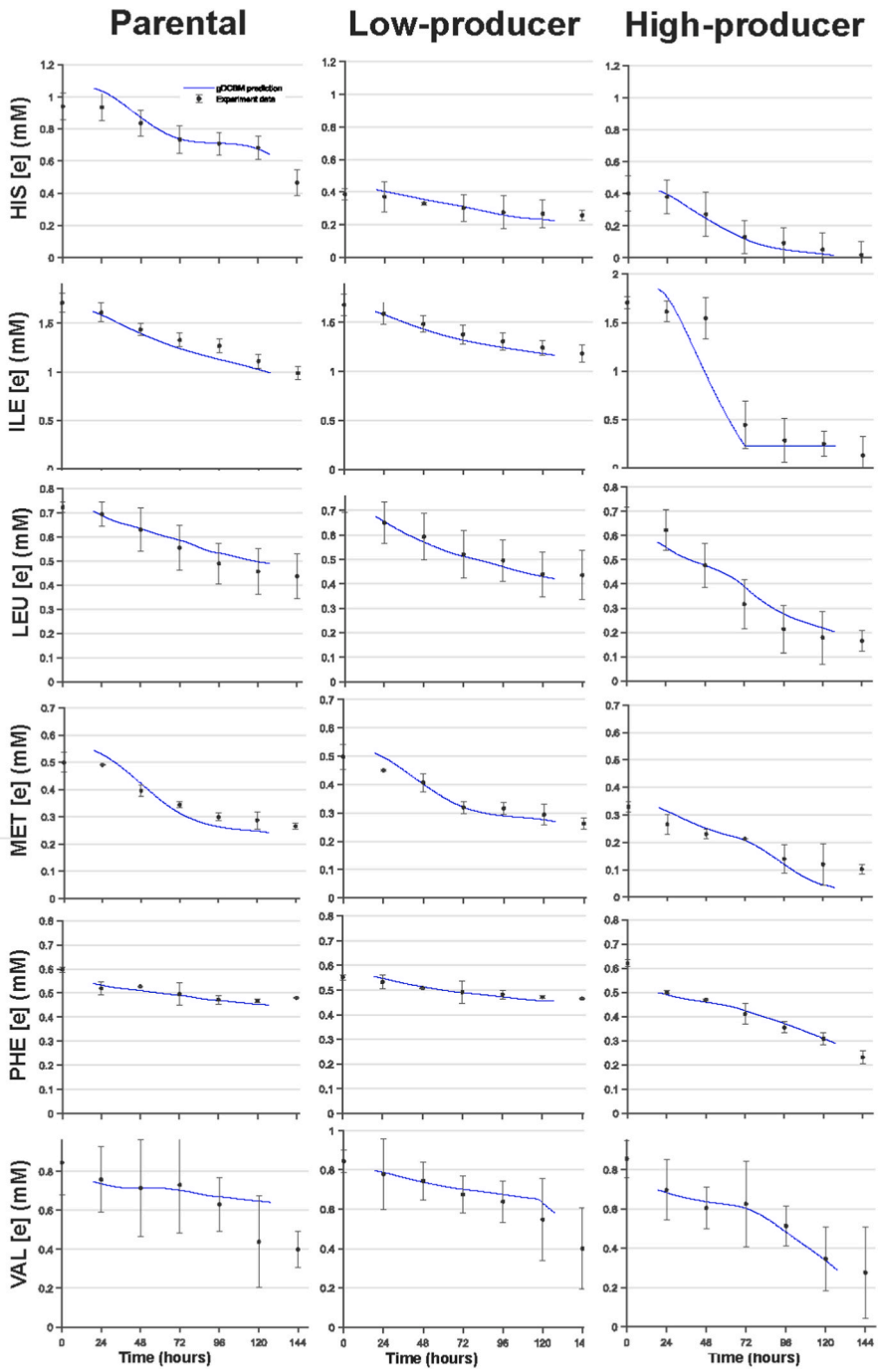

Fig. 6. Concentrations of the extracellular metabolites: Essential amino acids The rows reflect essential amino acid concentrations for which measurements were obtained, and the columns represent parental, low-producer, and high-producer clones. The blue lines reflect the gDCBM prediction of the concentrations, while the error bars reveal the experimental data.

increase in its demand from the intracellular environment.

3.8. Intracellular flux predictions

For the sake of brevity, we show in Fig. 8 five reactions from upper glycolysis and pentose phosphate pathway to show the ability of the framework to model intracellular reactions. Noteworthy is the demonstration of the optimal points along with the alternate optima range, which both addresses the well-known problem of FBA, namely, appearance of more than one optimum solution and shows that although some reactions work in a certain direction, but they can also work in other directions. For reaction HEX1 we observe that there are fractures in the optimal path passing zero activity, these fractures indicate the existence of different ways to convert glucose to g6p and are also a function of the sequential optimization method discussed in the Method section indicating a sudden change in the solution compared to the neighbouring points. This refers to how the answer is calculated step by step and that the answer of the equation at each point is independent of the previous or next point. The results show that at the beginning of the culture time the range of optimal alternative points is very narrow but it widens from the middle of the culture time. While for the high-producer clone this expansion coincides with the switch to the non-growth phase, it is not clear to the authors what is the reason for this change in the other two clones. We observed that in most of the intracellular flux

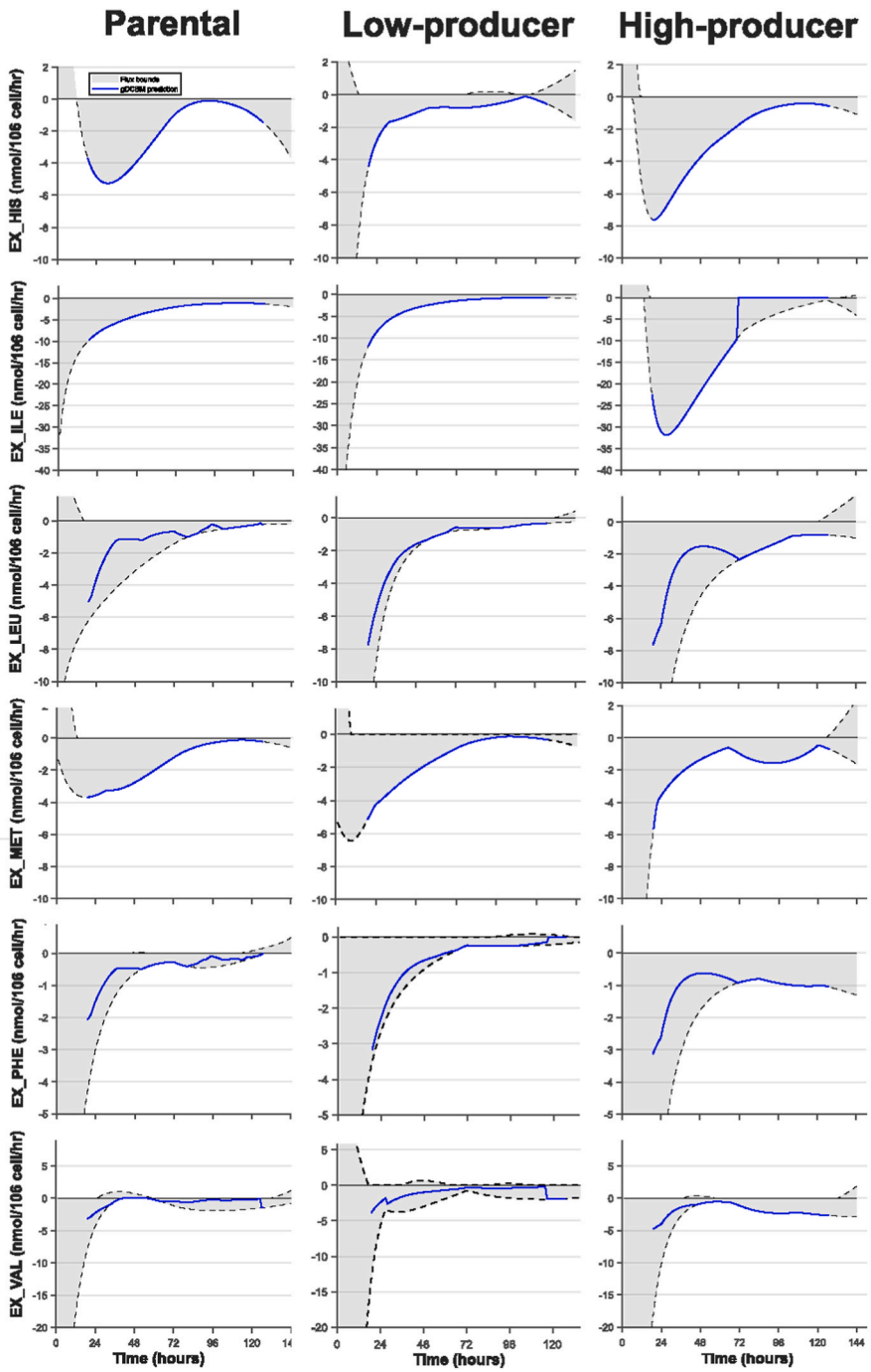

Fig. 7. Specific uptake or secretion rates: Essential amino acids The columns correspond to the parental, low-producer, and high-producer clones, respectively, and the rows to essential amino acids for which measurements were available. The blue lines reflect the gDCBM prediction of the specific rates, while the shaded areas show allowed bounds for the specific rates.

predictions large bands are obtained for the reactions. This shows that the restrictions were not enough, especially when a reaction is further from the exchange reactions or there are more than one way of exchanging material in and out of the cell. This pattern also points to the inherent robustness of the cell by having several routes and it shows why inactivation of single enzymes is not enough to navigate metabolic flux.

Several important aspects of metabolism such as enzyme regulation cannot be covered by this framework. In fact, the ability to model genome-scale phenotype of reactions was achieved in trade-off with losing the ability to study kinetic regulations. Thus, this study is in a sense complementary to the previous study conducted in our group which was focused on the development of a dynamic kinetic model for the same biosystem (Robitaille et al., 2015; Ghorbaniaghdam et al., 2014). Some intracellular flux predictions for example for the fluxes stemming from pyruvate indicates either inactivity or activity at the lower (upper) bound of the fluxes, it is in contrary to our findings with a reduced model of the same system (Ghorbaniaghdam et al., 2014). We justify that this happens because of the inclusion of pyruvate in four compartments (extracellular, cytoplasm, mitochondria and peroxisome) participating in a total of 30 reactions. This many degree of freedom for the mass balance on pyruvate may cause some false inactive fluxes and some unrealistically large fluxes. It points to the necessity of collecting more data such as carbon labeling data for further constraining the model and therefore navigating the flux into plausible reactions.

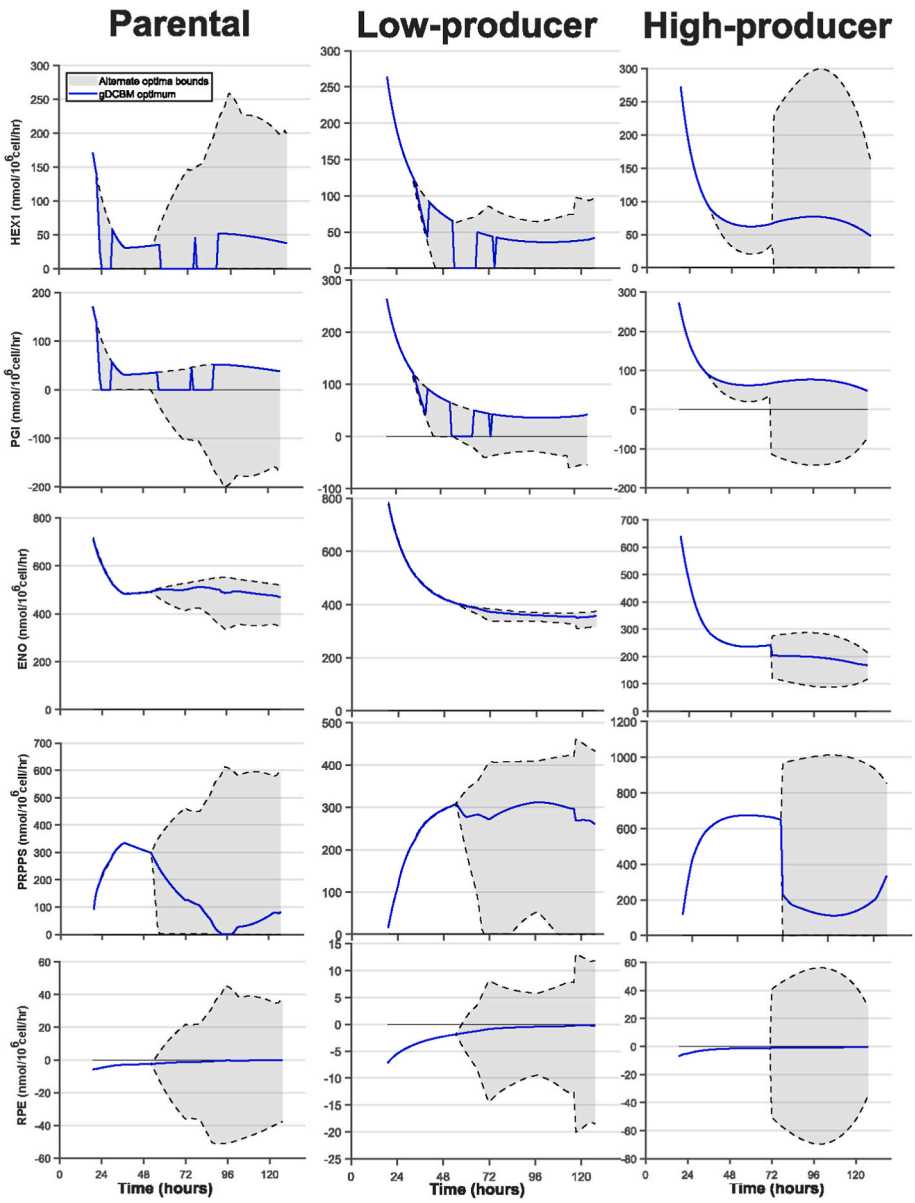

Fig. 8. Selected intracellular fluxes dynamics The blue lines indicate the optimum flux estimation and the shaded area shows the alternate optima bounds calculated for each flux based on FVA. HEX1: Hexokinase, PGI: Glucose-6-phosphate isomerase, ENO: Enolase, PRPPS: Phosphoribosylpyrophosphate synthetase, RPE: Ribulose 5-phosphate 3-epimerase.

4. Conclusion

In this work we built a modelling approach named gDCBM upon two main principles: (i) metabolic network dynamics is key to describe cell physiology, and (ii) optimality hypotheses support generating predictions in cell culture. We proposed a gDCBM framework in which a metabolic network for the CHO cell line was selected, bound by cell culture specific uptake rates, and then tuned to predict growth dynamics with a 1-h temporal resolution. In fact, cell internal metabolism was linked to the dynamic of change for external moieties. This global genome-wide understanding of mammalian cell metabolism was then used to investigate differences in clonal variations of CHO cell lines. The model showed being able to successfully predict the time trajectory of all available experimental measurements except for the model antibody, which was produced in small quantities and on flux levels that were significantly lower than other fluxes. We believe that the proposed mechanistic gDCBM metabolic network modelling technique can help to overcome some of the current challenges in *in-vitro* and *in-silico* bioprocess optimization. This technique is likely to benefit complex organisms like mammalian cells, which can absorb a variety of diverse nutritional sources. With such a metabolic modelling framework, better applications for investigating cell metabolism and physiology, as well as media optimization and biomanufacturing control, may be achievable.

5. Software

All the calculations and computations were done using MATLAB R2020b (The Mathworks; Natick, MA, USA) as compiler. The computational algorithms are cited in the text and were implemented through developed scripts using glpk, gurobi, or CPLEX optimization solvers (academic licenses) (gnu.org/software/glpk/, gurobi.com, ibm.com/analytics/cplex-optimizer) and with borrowed functions from COBRA Toolbox library ((Heirendt et al., 2019)) and CellNetAnalyzer library of MATLAB functions. The computational demand of gDCBM for a system of 2132 reactions at 100 time points exceeded capability of a personal computer with Intel(r) Core(TM) i5-8250U CPU @ 1.60 GHz and 8 GB

RAM memory. Thus, the analysis were performed on remote high-performance computing (HPC) clusters of Compute Canada. It took 2 h to run the algorithm once on a single computation node with 12 CPU-workers and 20 GB RAM.

Authors' contributions

MY, Conceptualization, Data curation, Formal analysis, Investigation, Methodology, Software, Validation, Visualization, Writing - original draft, Writing - review editing; MJ, Conceptualization, Funding acquisition, Methodology, Project administration, Resources, Software, Supervision, Writing - original draft, Writing - review editing.

Funding

MJ received the NSERC (https://www.nserc-crsng.gc.ca/) Discovery Grant #RGPIN- 2019–05050. The funders had no role in study design, data collection and analysis, decision to publish, or preparation of the manuscript.

Author statement

The authors declare that they have no competing interests.

Declaration of competing interest

The authors declare that they have no competing interests.

Data availability

Data will be made available on request.

Appendix A. Supplementary data

Supplementary data to this article can be found online at https://doi.org/10.1016/j.ymben.2023.06.005.

References

Altamirano, C., Illanes, A., Casablancas, A., Gámez, X., Cairó, J.J., Gòdia, C., 2001. Analysis of CHO cells metabolic redistribution in a glutamate-based defined medium in continuous culture. Biotechnol. Prog. 17 (6), 1032–1041. https://doi.org/10.1021/bp0100981.

Altamirano, C., Illanes, A., Becerra, S., Cairó, J.J., Gòdia, F., 2006. Considerations on the lactate consumption by CHO cells in the presence of galactose. J. Biotechnol. 125 (4), 547–556. https://doi.org/10.1016/j.jbiotec.2006.03.023.

Antoniewicz, M.R., 2020. A guide to metabolic flux analysis in metabolic engineering: methods, tools and applications. Metab. Eng. https://doi.org/10.1016/j.ymben.2020.11.002.

Aoyama, M., Tada, M., Tatematsu, K.I., Hashii, N., Sezutsu, H., Ishii-Watabe, A., 2018. Effects of amino acid substitutions on the biological activity of anti-CD20 monoclonal antibody produced by transgenic silkworms (Bombyx mori). Biochem. Biophys. Res. Commun. 503 (4), 2633–2638. https://doi.org/10.1016/j.bbrc.2018.08.015.

Ataman, M., Hernandez Gardiol, D.F., Fengos, G., Hatzimanikatis, V., 2017. redGEM: systematic reduction and analysis of genome-scale metabolic reconstructions for development of consistent core metabolic models. PLoS Comput. Biol. 13 (7), e1005444 https://doi.org/10.1371/journal.pcbi.1005444.

Bailey, J.E., 1998. Mathematical modeling and analysis in biochemical engineering: past accomplishments and future opportunities. Biotechnol. Prog. 14 (1), 8–20. https://doi.org/10.1021/bp9701269.

Becker, S.A., Palsson, B.O., 2008. Context-specific metabolic networks are consistent with experiments. PLoS Comput. Biol. 4 (5), e1000082 https://doi.org/10.1371/journal.pcbi.1000082.

Bonarius, H.P.J., Hatzimanikatis, V., Meesters, K.P.H., de Gooijer, C.D., Schmid, G., Tramper, J., 1996. Metabolic flux analysis of hybridoma cells in different culture media using mass balances. Biotechnol. Bioeng. 50 (3), 299–318. https://doi.org/10.1002/(SICI)1097-0290(19960505)50:3¡299::AID-BIT9¿3.0.CO;2-B.

Calmels, C., McCann, A., Malphettes, L., Andersen, M.R., 2019. Application of a curated genome-scale metabolic model of CHO DG44 to an industrial fed-batch process. Metab. Eng. 51, 9–19. https://doi.org/10.1016/j.ymben.2018.09.009.

Chen, Y., McConnell, B.O., Gayatri Dhara, V., Mukesh Naik, H., Li, C.T., Antoniewicz, M. R., et al., 2019. An unconventional uptake rate objective function approach enhances applicability of genome-scale models for mammalian cells. npj Systems Biology and Applications 5 (1), 25. https://doi.org/10.1038/s41540-019-0103-6.

Cloutier, M., Chen, J., Tatge, F., McMurray-Beaulieu, V., Perrier, M., Jolicoeur, M., 2009. Kinetic metabolic modelling for the control of plant cells cytoplasmic phosphate. J. Theor. Biol. 259 (1), 118–131.

Cuthrell, J.E., Biegler, L.T., 1987. On the optimization of differential-algebraic process systems. AIChE J. 33 (8), 1257–1270. https://doi.org/10.1002/aic.690330804.

Erdrich, P., Steuer, R., Klamt, S., 2015. An algorithm for the reduction of genome-scale metabolic network models to meaningful core models. BMC Syst. Biol. 9, 48. https://doi.org/10.1186/s12918-015-0191-x.

Feist, A.M., Palsson, B.O., 2010. The biomass objective function. Curr. Opin. Microbiol. 13 (3), 344–349. https://doi.org/10.1016/j.mib.2010.03.003.

Fernandes de Sousa, S., Bastin, G., Jolicoeur, M., Vande Wouwer, A., 2016. Dynamic metabolic flux analysis using a convex analysis approach: application to hybridoma cell cultures in perfusion. Biotechnol. Bioeng. 113 (5), 1102–1112. https://doi.org/10.1002/bit.25879.

Gábor, A., Banga, J.R., 2015. Robust and efficient parameter estimation in dynamic models of biological systems. BMC Syst. Biol. 9 https://doi.org/10.1186/s12918-015-0219-2, 74–74.

Gašperšič, J., Kastelic, M., Novak, U., Likozar, B., 2018. Metabolic network modelling of Chinese hamster ovary (CHO) culture bioreactors operated as microbial cell factories. Acta Chim. Slov. 65 (4), 769–786. https://doi.org/10.17344/acsi.2018.4591.

Ghorbaniaghdam, A., Chen, J., Henry, O., Jolicoeur, M., 2014. Analyzing clonal variation of monoclonal antibody-producing CHO cell lines using an in silico metabolomic platform. PLoS One 9 (3), e90832. https://doi.org/10.1371/journal.pone.0090832.

Hammond, S., Swanberg, J.C., Kaplarevic, M., Lee, K.H., 2011. Genomic sequencing and analysis of a Chinese hamster ovary cell line using Illumina sequencing technology. BMC Genom. 12, 67. https://doi.org/10.1186/1471-2164-12-67.

Hefzi, H., Ang, K.S., Hanscho, M., Bordbar, A., Ruckerbauer, D., Lakshmanan, M., et al., 2016. A consensus genome-scale reconstruction of Chinese hamster ovary cell metabolism. Cell Syst 3 (5). https://doi.org/10.1016/j.cels.2016.10.020.

Heirendt, L., Arreckx, S., Pfau, T., Mendoza, S.N., Richelle, A., Heinken, A., et al., 2019. Creation and analysis of biochemical constraint-based models using the COBRA Toolbox v.3.0. Nat. Protoc. 14 (3), 639–702. https://doi.org/10.1038/s41596-018-0098-2.

Kim, J.Y., Kim, Y.G., Lee, G.M., 2012. CHO cells in biotechnology for production of recombinant proteins: current state and further potential. Appl. Microbiol. Biotechnol. 93 (3), 917–930. https://doi.org/10.1007/s00253-011-3758-5.

Kotidis, P., Jedrzejewski, P., Sou, S.N., Sellick, C., Polizzi, K., Del Val, I.J., et al., 2019. Model-based optimization of antibody galactosylation in CHO cell culture. Biotechnol. Bioeng. 116 (7), 1612–1626. https://doi.org/10.1002/bit.26960.

Lugar, D.J., Mack, S.G., Sriram, G., 2021. NetRed, an algorithm to reduce genome-scale metabolic networks and facilitate the analysis of flux predictions. Metab. Eng. 65, 207–222. https://doi.org/10.1016/j.ymben.2020.11.003.

Mahadevan, R., Schilling, C.H., 2003. The effects of alternate optimal solutions in constraint-based genome-scale metabolic models. Metab. Eng. 5 (4), 264–276. https://doi.org/10.1016/j.ymben.2003.09.002.

Mahadevan, R., Edwards, J.S., Doyle, F.J., 2002. Dynamic flux balance analysis of diauxic growth in Escherichia coli. Biophys. J. 83 (3), 1331–1340.

Meadows, A.L., Karnik, R., Lam, H., Forestell, S., Snedecor, B., 2010. Application of dynamic flux balance analysis to an industrial Escherichia coli fermentation. Metab. Eng. 12 (2), 150–160.

Nolan, R.P., Lee, K., 2011. Dynamic model of CHO cell metabolism 13 (1), 108–124. https://doi.org/10.1016/j.ymben.2010.09.003.

Nolan, R.P., Lee, K., 2012. Dynamic model for CHO cell engineering. J. Biotechnol. 158 (1–2), 24–33. https://doi.org/10.1016/j.jbiotec.2012.01.009.

Nyberg, G.B., Balcarcel, R.R., Follstad, B.D., Stephanopoulos, G., Wang, D.I., 1999. Metabolism of peptide amino acids by Chinese hamster ovary cells grown in a complex medium. Biotechnol. Bioeng. 62 (3), 324–335.

Orth, J.D., Thiele, I., Palsson, B.Ø., 2010. What is flux balance analysis? Nat. Biotechnol. 28 (3), 245–248.

Pacheco, M.P., Sauter, T., 2018. The FASTCORE family: for the fast reconstruction of compact context-specific metabolic networks models. Methods Mol. Biol. 1716, 101–110. https://doi.org/10.1007/978-1-4939-7528-0_4.

Porubsky, V.L., Goldberg, A.P., Rampadarath, A.K., Nickerson, D.P., Karr, J.R., Sauro, H. M., 2020. Best practices for making reproducible biochemical models. Cell Syst 11 (2), 109–120. https://doi.org/10.1016/j.cels.2020.06.012.

Quek, L.E., Dietmair, S., Kromer, J.O., Nielsen, L.K., 2010. Metabolic flux analysis in mammalian cell culture. Metab. Eng. 12 (2), 161–171. https://doi.org/10.1016/j.ymben.2009.09.002.

Richelle, A., Chiang, A.W.T., Kuo, C.C., Lewis, N.E., 2019. Increasing consensus of context-specific metabolic models by integrating data-inferred cell functions. PLoS Comput. Biol. 15 (4), e1006867 https://doi.org/10.1371/journal.pcbi.1006867.

Robitaille, J., Chen, J., Jolicoeur, M., 2015. A single dynamic metabolic model can describe mAb producing CHO cell batch and fed-batch cultures on different culture media. PLoS One 10 (9), e0136815. https://doi.org/10.1371/journal.pone.0136815.

Savinell, J.M., Palsson, B.O., 1992. Optimal selection of metabolic fluxes for in vivo measurement. II. Application to Escherichia coli and hybridoma cell metabolism. J. Theor. Biol. 155 (2), 215–242. https://doi.org/10.1016/s0022-5193(05)80596-x.

Schellenberger, J., Que, R., Fleming, R.M., Thiele, I., Orth, J.D., Feist, A.M., et al., 2011. Quantitative prediction of cellular metabolism with constraint-based models: the COBRA Toolbox v2. 0. Nat. Protoc. 6 (9), 1290. https://doi.org/10.1038/nprot.2011.308.

Schuetz, R., Zamboni, N., Zampieri, M., Heinemann, M., Sauer, U., 2012. Multidimensional optimality of microbial metabolism. Science 336 (6081), 601–604. https://doi.org/10.1126/science.1216882.

Sha, S., Huang, Z.R., Wang, Z., Yoon, S., 2018. Mechanistic modeling and applications for CHO cell culture development and production. Curr. Opin. Chem. Eng. 22, 54–61. https://doi.org/10.1016/j.coche.2018.08.010.

Sheikh, K., Forster, J., Nielsen, L.K., 2005. Modeling hybridoma cell metabolism using a generic genome-scale metabolic model of Mus musculus. Biotechnol. Prog. 21 (1), 112–121. https://doi.org/10.1021/bp0498138.

Sheikholeslami, Z., Jolicoeur, M., Henry, O., 2013. The impact of the timing of induction on the metabolism and productivity of CHO cells in culture. Biochem. Eng. J. 79, 162–171. https://doi.org/10.1016/j.bej.2013.07.015.

Sheikholeslami, Z., Jolicoeur, M., Henry, O., 2014. Elucidating the effects of postinduction glutamine feeding on the growth and productivity of CHO cells. Biotechnol. Prog. 30 (3), 535–546. https://doi.org/10.1002/btpr.1907.

Stephanopoulos, G., Aristidou, A.A., Nielsen, J., 1998. Metabolic Engineering: Principles and Methodologies. Academic press.

Széliová, D., Ruckerbauer, D.E., Galleguillos, S.N., Petersen, L.B., Natter, K., Hanscho, M., et al., 2020. What CHO is made of: variations in the biomass composition of Chinese hamster ovary cell lines. Metab. Eng. 61, 288–300. https://doi.org/10.1016/j.ymben.2020.06.002.

Szeliova, D., Stor, J., Thiel, I., Weinguny, M., Hanscho, M., Lhota, G., et al., 2021. Inclusion of maintenance energy improves the intracellular flux predictions of CHO. PLoS Comput. Biol. 17 (6), e1009022 https://doi.org/10.1371/journal.pcbi.1009022.

Tefagh, M., Boyd, S.P., 2020. SWIFTCORE: a tool for the context-specific reconstruction of genome-scale metabolic networks. BMC Bioinf. 21 (1), 140. https://doi.org/10.1186/s12859-020-3440-y.

Thiele, I., Palsson, B.O., 2010. A protocol for generating a high-quality genome-scale metabolic reconstruction. Nat. Protoc. 5 (1), 93–121. https://doi.org/10.1038/nprot.2009.203.

Type [;]. Available from: https://go.drugbank.com/drugs/DB00073.

Varma, A., Palsson, B.O., 1994. Stoichiometric flux balance models quantitatively predict growth and metabolic by-product secretion in wild-type Escherichia coli W3110. Appl. Environ. Microbiol. 60 (10), 3724–3731.

Xie, L.Z., Wang, D.I.C., 1996. Material balance studies on animal cell metabolism using a stoichiometrically based reaction network. Biotechnol. Bioeng. 52 (5), 579–590. https://doi.org/10.1002/(Sici)1097-0290(19961205)52.

Yasemi, M., Jolicoeur, M., 2021. Modelling cell metabolism: a review on constraint-based steady-state and kinetic approaches. Processes 9 (2). https://doi.org/10.3390/pr9020322.

Yeo, H.C., Hong, J., Lakshmanan, M., Lee, D.Y., 2020. Enzyme capacity-based genome scale modelling of CHO cells. Metab. Eng. 60, 138–147. https://doi.org/10.1016/j.ymben.2020.04.005.

Zamorano, F., Wouwer, A.V., Bastin, G., 2010. A detailed metabolic flux analysis of an underdetermined network of CHO cells. J. Biotechnol. 150 (4), 497–508. https://doi.org/10.1016/j.jbiotec.2010.09.944.

Zupke, C., Stephanopoulos, G., 1994. Modeling of isotope distributions and intracellular fluxes in metabolic networks using atom mapping matrixes. Biotechnol. Prog. 10 (5), 489–498. https://doi.org/10.1021/bp00029a006.

Zupke, C., Stephanopoulos, G., 1995. Intracellular flux analysis in hybridomas using mass balances and in vitro 13C nmr. Biotechnol. Bioeng. 45 (4), 292–303. https://doi.org/10.1002/bit.260450403.